Medical Physics
The International Journal of Medical Physics Research and Practice

Whole-remnant and maximum-voxel SPECT/CT dosimetry in 131I-NaI treatments of differentiated thyroid cancer

Pablo Mínguez, Glenn Flux, José Genollá, Alejandro Delgado, Emilia Rodeño, and Katarina Sjögreen Gleisner

Citation: Medical Physics **43**, 5279 (2016); doi: 10.1118/1.4961742
View online: http://dx.doi.org/10.1118/1.4961742
View Table of Contents: http://scitation.aip.org/content/aapm/journal/medphys/43/10?ver=pdfcov
Published by the American Association of Physicists in Medicine

Whole-remnant and maximum-voxel SPECT/CT dosimetry in ^{131}I-NaI treatments of differentiated thyroid cancer

Pablo Mínguez[a)]
Department of Medical Radiation Physics, Lund University, Lund 22185, Sweden and Department of Medical Physics, Gurutzeta/Cruces University Hospital, Barakaldo 48903, Spain

Glenn Flux
Joint Department of Physics, Royal Marsden NHS Foundation Trust and Institute of Cancer Research, Sutton SM2 5PT, United Kingdom

José Genollá, Alejandro Delgado, and Emilia Rodeño
Department of Nuclear Medicine, Gurutzeta/Cruces University Hospital, Barakaldo 48903, Spain

Katarina Sjögreen Gleisner
Department of Medical Radiation Physics, Lund University, Lund 22185, Sweden

(Received 12 April 2016; revised 8 August 2016; accepted for publication 13 August 2016; published 6 September 2016)

Purpose: To investigate the possible differences between SPECT/CT based whole-remnant and maximum-voxel dosimetry in patients receiving radio-iodine ablation treatment of differentiated thyroid cancer (DTC).
Methods: Eighteen DTC patients were administered 1.11 GBq of ^{131}I-NaI after near-total thyroidectomy and rhTSH stimulation. Two patients had two remnants, so in total dosimetry was performed for 20 sites. Three SPECT/CT scans were performed for each patient at 1, 2, and 3–7 days after administration. The activity, the remnant mass, and the maximum-voxel activity were determined from these images and from a recovery-coefficient curve derived from experimental phantom measurements. The cumulated activity was estimated using trapezoidal-exponential integration. Finally, the absorbed dose was calculated using *S*-values for unit-density spheres in whole-remnant dosimetry and *S*-values for voxels in maximum-voxel dosimetry.
Results: The mean absorbed dose obtained from whole-remnant dosimetry was 40 Gy (range 2–176 Gy) and from maximum-voxel dosimetry 34 Gy (range 2–145 Gy). For any given patient, the activity concentrations for each of the three time-points were approximately the same for the two methods. The effective half-lives varied ($R = 0.865$), mainly due to discrepancies in estimation of the longer effective half-lives. On average, absorbed doses obtained from whole-remnant dosimetry were 1.2 ± 0.2 (1 SD) higher than for maximum-voxel dosimetry, mainly due to differences in the *S*-values. The method-related differences were however small in comparison to the wide range of absorbed doses obtained in patients.
Conclusions: Simple and consistent procedures for SPECT/CT based whole-volume and maximum-voxel dosimetry have been described, both based on experimentally determined recovery coefficients. Generally the results from the two approaches are consistent, although there is a small, systematic difference in the absorbed dose due to differences in the *S*-values, and some variability due to differences in the estimated effective half-lives, especially when the effective half-life is long. Irrespective of the method used, the patient absorbed doses obtained span over two orders of magnitude.
 [http://dx.doi.org/10.1118/1.4961742]

Key words: differentiated thyroid carcinoma, ^{131}I-NaI, thyroid bed remnants, dosimetry

1. INTRODUCTION

Administration of ^{131}I-NaI for postoperative ablation of thyroid remnants for the treatment of differentiated thyroid cancer (DTC) has been commonly accepted since the 1940s.[1] Activities of 1.11–3.7 GBq are usually administered[2] and a number of studies have dealt with the outcome of the treatment.[3–10] The absorbed dose to thyroid remnants has been investigated[11–20] leading to a wide range of mean values per unit of administered activity, e.g., 28,[18] 65,[19] 93,[13,14] and 322 Gy/GBq.[15] Maxon *et al.*,[11] O'Connell *et al.*,[14] and Flux *et al.*,[18] correlated the absorbed dose to the outcome of the treatment, reporting values of absorbed dose to thyroid remnants above which there is a significant probability of successful ablation. Maxon *et al.*[11] reported a value of 300 Gy, whereas O'Connell *et al.*[14] and Flux *et al.*,[18] gave more similar values of 60 and 49 Gy, respectively.

A plausible explanation for the wide range of the absorbed doses reported, are differences in methodology for imaging, activity quantification, and dosimetry. In previous studies, imaging modalities included rectilinear scans with one head[11,13,15] or two heads,[14] gamma-camera imaging in

planar[12,16,19] or SPECT acquisition mode,[18] and PET/CT scanning.[17,20] Dosimetry has been based on tracer studies of ^{131}I[11,13,15,16] or ^{124}I,[17,20] or therapy studies.[12,14,16,18,19] In most cases at least three scans have been acquired, although one study reported up to nine scans.[12] The timing of the scans has differed, and the last imaging time-point has varied between 3 and 14 days after administration. For determination of the cumulated activity, different approaches have been followed, such as using an effective half-life retrieved from the literature,[17] a monoexponential time-activity curve determined from data,[14,15] a curve including several phases,[12,19,20] or a trapezoidal integration and a monoexponential curve for extrapolation beyond the last data point.[16,18] Methods used for determination of the thyroid remnants mass have also varied and mass has been estimated using the cross-sectional area in planar images,[11,13–16,19] anterior- and lateral-view imaging,[12] or iterative thresholding methods.[14,17,18,20] Usually the whole-remnant has been considered to perform dosimetry. However, Flux *et al.*[18] introduced maximum-voxel dosimetry, i.e., dosimetry using the voxel of maximum counts in SPECT images.

^{131}I SPECT/CT imaging is now widely available. The absorbed dose to thyroid remnants can therefore be performed with whole-volume or maximum-voxel based methods. The aim of this study was to investigate the possible differences between these two approaches. For this purpose, a straightforward calibration-based procedure was developed, based on SPECT/CT imaging and basic quality-control phantoms. The recovery-coefficient curve derived in this method was applied for both whole-volume and maximum-voxel dosimetry in 20 sites of radio-iodine uptake in 18 patients.

2. METHODS

2.A. Data collection and processing

2.A.1. Patient data and imaging

Data included 18 patients (14 female and four male) treated for low-risk DTC (Refs. 1 and 2) with 1.11 GBq of ^{131}I-NaI after stimulation with rhTSH. In two patients, there were two remnants with radio-iodine uptake, so in total dosimetry of 20 sites was performed. Prior to therapy, patients had undergone a near-total or complete thyroidectomy. After radio-iodine administration, patients remained 24 h as inpatients and were released when the dose-rate at 1 m was below 40 mSv/h, according to recommendations of the IAEA.[21] Informed consent was obtained from all patients.

Three SPECT/CT acquisitions centered on the neck region were performed for each patient. Imaging times were at 1, 2, and 3–7 days after administration. The time of the third acquisition varied because acquisitions were not performed during weekends and depending on the availability of the gamma camera. SPECT/CT acquisitions were performed employing a dual-head General Electric (GE, Fairfield, CT, USA) Infinia Hawkeye gamma camera, with a crystal thickness of 9.5 mm and equipped with High-Energy General-Purpose collimators. A helical CT of pitch 1.9 was performed using 120 kVp (the lowest available value), 2 mA, and a rotation velocity of 2.6 rpm. The CT was used for SPECT attenuation correction. SPECT projections were acquired in 60 angles. For the first two patients, the projection time was 60 s, while for the other patients it was 45 s due to limited availability of the gamma camera. A matrix size of 128×128 was used, and a voxel size of 0.442^3 cm^3. A photopeak energy window centered at 364 keV and 20% in width was used. For scatter correction, a dual energy window method implemented by GE was performed, with an additional window centered at 297 keV and 20% in width. SPECT image reconstruction was performed using the ordered subsets expectation maximization algorithm in a Xeleris work station of GE, with two iterations and ten subsets, applying a Butterworth filter with critical frequency 0.5 cycles/cm and power 10 (order 5). Analysis of SPECT images was performed using the ImageJ program (NIH, Bethesda, MD, USA). Figure 1 shows an example of patient SPECT images from three sequential time-points.

2.A.2. Phantom measurements and simulations

Two phantoms were used for calibration and method development: a cylindrically shaped phantom of 4 l (diameter 15.5 cm and height 21.2 cm) filled with an aqueous solution of ^{131}I-NaI; and the IEC-Standard 61675-1 image-quality phantom[22] in which the six spheres of volumes 0.5, 1.2, 2.6, 5.6, 11.5, and 26.5 cm^3 were filled with an aqueous solution of ^{131}I-NaI. The activity concentration in the spheres ranged between 0.4 and 2.3 MBq/cm^3, as measured in a dose calibrator Capintec CRC®-15R (Capintec, Inc., Ramsey, NJ, USA).

SPECT/CT acquisition of the elliptically shaped phantom was performed using the same acquisition parameters as for patients, and the total number of counts in a volume corresponding to the physical phantom volume was determined. This value was divided by the acquisition time and the contained activity, giving the calibration factor, ε, in unit cps/MBq. For the IEC phantom measurements, four SPECT/CT acquisitions were performed using the same parameters as used for patients with the exception of the time per projection, which was either 10 or 15 s. The results of the reconstructions of the four acquisitions were averaged in order to reduce the uncertainty of the acquisitions.

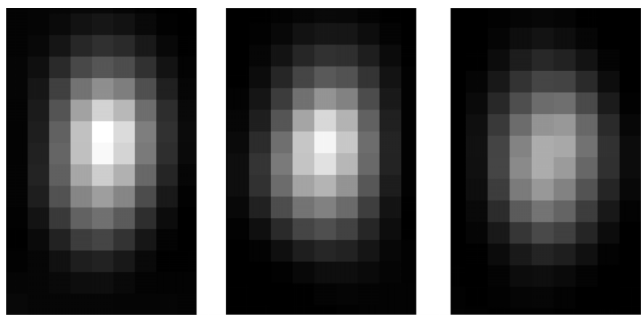

FIG. 1. The central part of reconstructed SPECT images focused on the site with radio-iodine uptake for one patient. Images shown, from left to right, were acquired at 1, 2, and 4 days after administration and are in the same greyscale.

In addition to phantom measurements, computer simulations of imaging were performed. Voxelized, approximately spherically shaped, objects with uniform activity concentration were defined centrally in 3D image matrices. To mimic effects of limited spatial resolution, these images were convolved with a 3D Gaussian function whose full-width at half maximum (FWHM) was defined to three, four, and five times the voxel dimensions of the patient SPECT images, thus corresponding to 13.3, 17.7, and 22.1 mm, respectively. These FWHMs were selected to mimic the reconstructed resolution of real gamma camera systems. For the camera system used herein, the FWHM of the point-spread function (PSF) was measured to be 19 mm. These simulations were performed in Interactive Data Language, version 8.4 (Exelis Visual Information Solutions, Inc.).

2.B. Dosimetry of sites with radio-iodine uptake

2.B.1. Recovery coefficients for homogenous spherical objects

In order to quantify the activity concentration in small volumes, a common approach is to apply recovery coefficients to compensate for effects of limited resolution. Appendix A shows the method followed to determine the volume of spherical objects with homogeneous activity concentration by using recovery coefficients.

2.B.2. Whole-volume dosimetry (Method 1)

The consistency between measurements in the elliptically shaped phantom and the IEC phantom spheres was first checked. For the four acquisitions of the IEC phantom, the counts originating from each sphere were determined by drawing a rough VOI around the sphere and applying a 5% threshold to exclude counts from septal penetration and scatter. The sphere activity was then determined by dividing the total counts by the acquisition time and the calibration factor, ε, determined from the 4 l-calibration phantom. Using this procedure the sphere activities could be determined to within 10% from the inserted activities measured in the dose calibrator.

The whole volume of the site of radio-iodine uptake was considered for dosimetry. To determine the activity from patient SPECT images, the sites were roughly delineated with a margin, and a threshold of 30% was applied to discriminate against activity in surrounding tissues. Thresholds of 20% and 40% were also investigated, obtaining similar results, and a value of 30% was chosen as a compromise to avoid background counts while maintaining a sufficient count level. The total count rate, C_{30}, was determined and the site activity, A_s, was calculated according to

$$A_s = \frac{C_{30}}{\varepsilon f_{30}}. \tag{1}$$

The parameter f_{30} was introduced to compensate for the loss of count rate resulting from applying the 30% threshold and was determined based on the IEC phantom spheres as the ratio of the total count rates when using a 30% threshold to that using a 5% threshold. For the IEC phantom data, it was observed that in the volume range between 0.5 and 11.5 cm^3 this ratio was approximately constant and was obtained to be 0.59 ± 0.03 (1 SD). For comparison, the f_{30} obtained from the simulated sphere data were 0.61 ± 0.03, 0.59 ± 0.01, and 0.58 ± 0.01, for FWHMs of 13.3, 17.7, and 22.1 mm, respectively.

The activity A_s was determined for each of the consecutive SPECT images, and the cumulated activity $\tilde{A}_s$ was calculated by trapezoidal integration up to the last time-point, and thereafter assuming a monoexponentially decaying activity retention with an effective half-life determined from previous time-points.[16,18]

The site volume, v_s, was determined as described in Appendix A, Eq. (A5), with v_s in place of v_o,

$$v_s = RC(v_{a,s}) \cdot v_{a,s}. \tag{2}$$

The apparent site volume, $v_{a,s}$, was determined from patient SPECT images. However, because of the background count rate in surrounding tissues Eq. (A4) was less suited and $v_{a,s}$ was instead estimated following

$$v_{a,s} = \Delta v \frac{C_{30}}{c_m f_{30}}. \tag{3}$$

Each of the three SPECT images was evaluated, and the mean $v_{a,s}$ was calculated. The volume of the radio-iodine-accumulating sites was then determined using Eq. (2), with an RC determined for the mean $v_{a,s}$.

The whole-remnant absorbed dose, D_1, was determined as

$$D_1 = \tilde{A}_s S_{s \leftarrow s}(v_s)/\rho_{\text{thyr}}, \tag{4}$$

where $S_{s \leftarrow s}$ values in unit Gy MBq^{-1} h^{-1} were obtained using a function $S_{s \leftarrow s} = 0.110 \times v_s^{-0.974}$, which was derived by interpolation of values for unit-density spheres.[23] The mass density was also taken into consideration[24] and was considered to be that of thyroid tissue (1.05 g/cm^3).[25]

2.B.3. Maximum-voxel dosimetry (Method 2)

For patient SPECT images, the activity per voxel, A_{vx}, was estimated (see Appendix C) according to

$$A_{\text{vx}} = \frac{1}{\varepsilon} \frac{c_m}{\text{RC}(v_{a,s})}. \tag{5}$$

The cumulated activity per voxel, $\tilde{A}_{\text{vx}}$, was calculated by curve-fitting and integration according to the trapezoidal-exponential method described above. The maximum-voxel absorbed dose, D_2, was determined following

$$D_2 = \tilde{A}_{\text{vx}} S_{\text{vx} \leftarrow \text{vx}} \frac{\rho_{\text{tis}}}{\rho_{\text{thyr}}}, \tag{6}$$

where $S_{\text{vx} \leftarrow \text{vx}}$ was valid for the voxel size (a cubic voxel of side 0.442 cm), originally given[26] for soft tissue mass density, ρ_{tis}, of 1.04 g/cm^3. The factor $\rho_{\text{tis}}/\rho_{\text{thyr}}$ was introduced to compensate for differences in mass density[24] to that of thyroid (1.05 g/cm^3).[25] The density-scaled voxel S-value equaled 1.070 Gy/MBq h.

3. RESULTS

Data from patient studies are presented as mean value ±1 SD (range, first quartile, median value, third quartile). Values given in brackets are in the same unit as the mean.

The mean value of the mass of sites with ^{131}I uptake in all patients was (3.9 ± 2.2) g (1.3–9.1, 2.4, 3.0, 5.3). At 1 day after administration, the remaining activity in these sites, determined using Method 1, and the remaining activity per voxel, determined using Method 2, were (6.0 ± 4.0) MBq (1.0–13.6, 3.2, 5.0, 9.1) and (0.19 ± 0.18) MBq (0.02–0.75, 0.05, 0.16, 0.23), respectively. Figure 2 shows the activity per mass at three times of SPECT/CT imaging, for Methods 1 and 2. The correlation coefficients R between results for both methods were very close to 1, with values obtained for the first, second, and third acquisitions of 0.994, 0.998, and 0.998, respectively.

The mean values of the effective half-lives obtained from Methods 1 and 2 were similar, with results obtained of (114 ± 51) h (36–193, 73, 101, 149) and (117 ± 48) h (36–193, 80, 113, 151), respectively. Figure 3 shows the effective half-lives from Methods 1 and 2, with a correlation coefficient of 0.865. The mean value of the cumulated activity concentration determined from Method 1 was also similar to that obtained from Method 2, with values of (356 ± 407) MBq h g^{-1} (17–1578, 84, 209, 495) and (350 ± 379) MBq h g^{-1} (16–1501, 83, 216, 563), respectively. The correlation coefficient for the cumulated activity concentration obtained from Methods 1 and 2 was 0.986.

Figure 4(A) shows the ratio, D_1/D_2, of the absorbed dose obtained from Methods 1 and 2 as function of the site mass as estimated using Method 1. The mean value of these ratios was obtained to be 1.2 ± 0.2. Figure 4(A) also shows the interval delimited by the mean value ±2 SDs. From the 20 values, 19 were within 2 SDs (95% of the values), which agreed with a qualitative investigation (not shown) where the distribution of the ratios was found to be close to a normal distribution. The point with a value outside 2 SDs corresponds to the patient with the highest ratio of the effective half-lives obtained from Methods 1 and 2. For comparison, Fig. 4(A) also includes the ratio of absorbed doses determined for the spheres of the IEC phantom, as function of the sphere mass. This ratio increased slightly with mass and was close to the mean-ratio value for patients, confirming that there was a small, but systematic difference between absorbed doses estimated using Methods 1 and 2. Figure 4(B) shows the absorbed dose ratio when the contribution to the cumulated activity from the extrapolated part, beyond the last data point, is excluded. The contribution of the extrapolated part to the total cumulated activity was between 3% and 76% for Method 1 and between 4% and 70% for Method 2. It is seen that the main cause of the variability between Methods 1 and 2 in Fig. 4(A) is the estimation of the effective half-life.

Figure 5 shows a cumulative histogram of the number of patients in whom different levels of absorbed doses to sites were reached from Methods 1 and 2, respectively. The mean absorbed doses obtained were (40 ± 46) Gy (2–176, 9, 23, 56) and (34 ± 37) Gy (2–145, 8, 21, 55), for Methods 1 and 2, respectively. Thus, although methodological differences appeared to exist, with Method 2 giving slightly lower values than Method 1, these differences were small in comparison to the wide range of absorbed doses given.

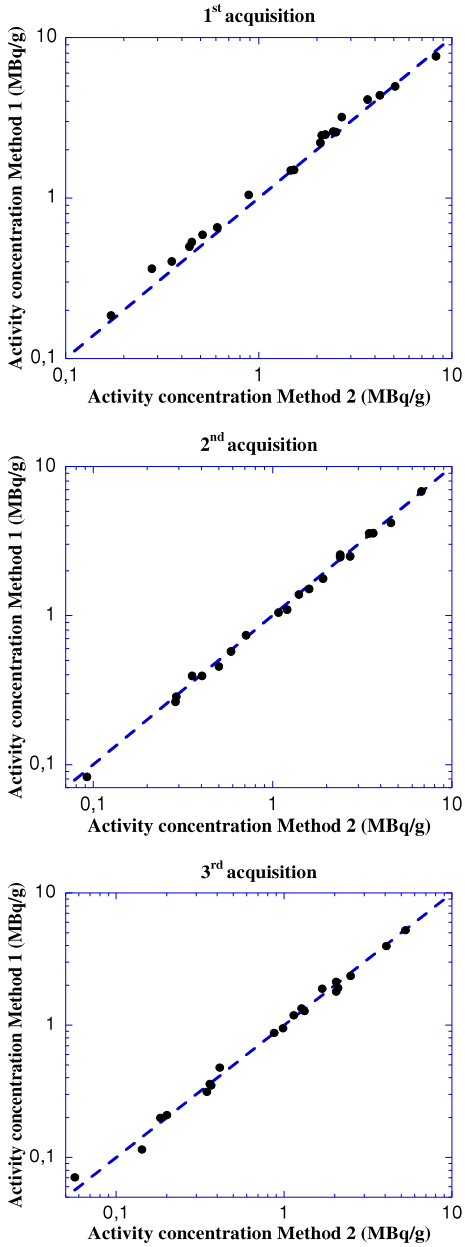

FIG. 2. The activity per mass obtained from Methods 1 (vertical axis) and 2 (horizontal axis), for the three SPECT/CT acquisitions performed for most patients at 1, 2, and 4 days after administration. The dashed line represents the line of identity. N.B. Axes are in logarithmic scale for purpose of visualization of data points.

4. DISCUSSION

Presently, most centers have the capability of ^{131}I SPECT/CT imaging. To promote dosimetry in DTC, it is of interest to develop methods that can be easily applied in currently used clinical platforms. Two approaches that have previously been

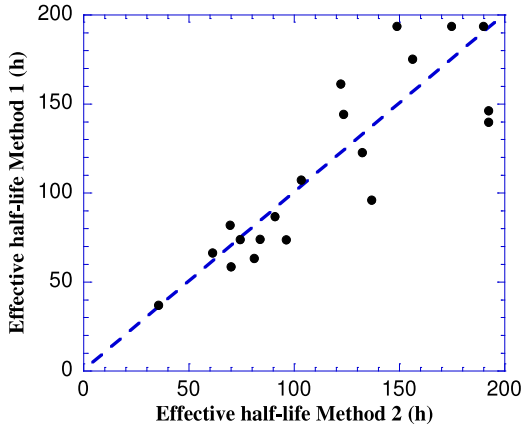

FIG. 3. Effective half-lives from Method 1 (vertical axis) and Method 2 (horizontal axis). The dashed is the line of identity.

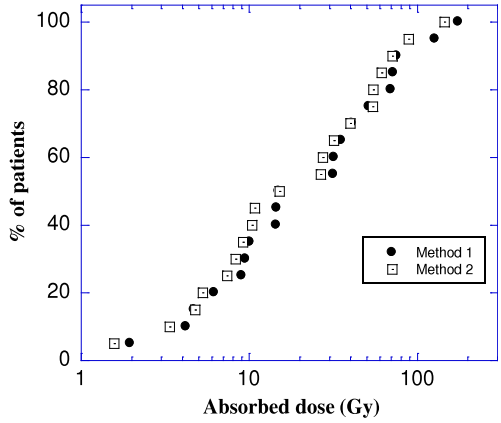

FIG. 5. Cumulative histogram of the percentage of patients that reached different absorbed doses to sites, as determined using Methods 1 and 2. N.B. The x-axis is on a logarithmic scale.

used for dosimetry are whole-volume and maximum-voxel based methods.[11,14,18] Practically, Method 2 has the advantage of not having to determine the total activity in the remnant by applying the thresholding procedure, but on the other hand, the remnant absorbed dose is underestimated since the contribution from neighboring voxels is disregarded. In this study, the possible differences and similarities between these methods have been investigated for 18 DTC patients and, in total, 20 sites of radio-iodine uptake.

Determination of small volumes from nuclear medicine images is severely limited by spatial resolution, and in context of DTC dosimetry, the mass estimation is thought to be the largest potential source of error.[11] Currently there is no standard method to determine the volume of sites of radio-iodine uptake following surgery. In this study, the volume is estimated using a procedure based on recovery coefficients and the concept of apparent volume, representing the imaged volume affected by spatial resolution. The procedure is robust in the sense that does not rely on the site border as reflected in the low-resolution SPECT images, and it can be easily implemented on clinical work stations and can thus be applied to all patients. The mean value of masses obtained was (3.9 ±2.2) g which is similar to previously reported values: 2.5 g,[12] 3.1 g,[14] 4.1 g,[15] 1.9 g,[16] and 6.6 g.[27] The obtained volumes may be considered high, but there are possible reasons for which the obtained masses are higher than that of the tissue left directly after surgery. Enlargement of thyroid tissue may occur as a consequence of radiation thyroiditis,[28] or due to stimulation with rhTSH.[29–31] Also, since patient acquisitions are made without immobilization devices, motion-induced blurring may produce an overestimated volume. The mass estimation is also affected by uncertainties in the RC-calibration curve (Fig. 7), mainly resulting from variability in the activities and volumes of the radioactive solution in the calibration phantom, and also the positioning of the phantom with regard to the gamma camera, affecting the reconstructed spatial resolution. Another methodological limitation is that the RC-calibration curve is determined from spherical objects with homogenous activity distributions and without surrounding activity, while the geometry of sites with ^{131}I uptake may be different and exhibit heterogeneities in the activity distributions. Also some background activity may be present, thus possibly affecting the true recovery coefficient. The assumption of spherical shapes is a starting point and is a commonly applied assumption,[32] and the activity concentration in tissues surrounding thyroid remnants is generally low. However for future studies, it is of

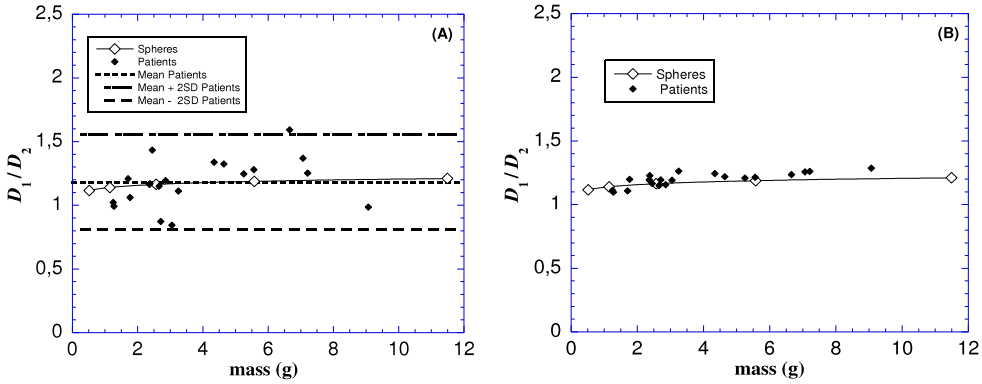

FIG. 4. (A) Ratio of absorbed doses when estimated using Methods 1 and 2 for patients as function of the site mass (black symbols), and for spheres in the IEC phantom (open connected symbols) as function of sphere mass. Horizontal lines show the mean value for patients and the interval defined by the mean value ±2 SDs. (B) The same ratios as in (A) when excluding the extrapolated exponential part in the integration of cumulated activity in sites of uptake.

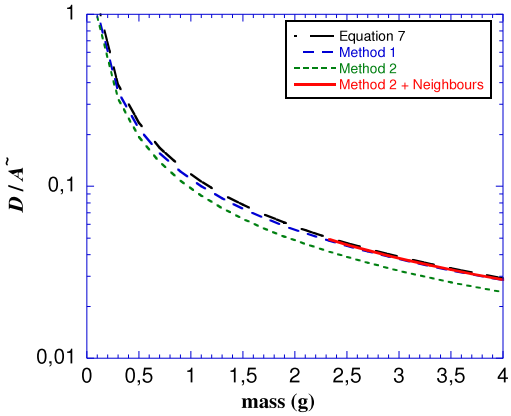

FIG. 6. Absorbed dose per unit of cumulated activity as function of mass, from Eq. (7), Method 1 [Eq. (4)], Method 2 [Eq. (6)], and Method 2 including neighbors (only for masses >2.3 g). N.B. The y-axis is plotted using a logarithmical scale.

interest to investigate these different sources of uncertainty in detail.

The obtained absorbed doses from the whole-volume and the maximum-voxel methods ranged between 2 and 176 Gy (mean 40 Gy) and 2 and 145 Gy (mean 34 Gy), respectively. As shown in Fig. 5, the difference obtained for each individual patient is small in relation to the wide range of absorbed doses. In Fig. 4, for the spheres of known volume and activity, it is seen that the ratio of absorbed doses from the two methods tends toward a value of approximately 1.2. Likewise for patient data, the mean ratio is 1.2. This difference can be explained by the S-values used for absorbed dose calculation. Figure 6 shows the absorbed dose per cumulated activity, as function of mass, from Eq. (4), based on unit density spheres, and Eq. (6), based on voxel S-values. In addition, values are shown for voxel S-values where the absorbed-dose contribution from neighboring voxels is taken into account, as provided in the study by Lanconelli *et al.*[26] For this last method, only masses higher than 2.3 g are considered, corresponding to 27 voxels including the 6 closest neighbors, the 12 second neighbors, and the 8 third neighbors. As a fourth source of comparison, the method given in guidelines for radio-iodine therapy of DTC from the European Association of Nuclear Medicine (EANM)[2] is included, where the equation for the absorbed dose to sites with ^{131}I uptake is the following:

$$D = \tilde{A}_s S_{\text{th}\leftarrow\text{th}} \frac{m_{\text{ref,th}}}{m_s}, \tag{7}$$

where $S_{\text{th}\leftarrow\text{th}}$ is the MIRD defined S-value for thyroid self-irradiation (5.652×10^{-3} Gy MBq^{-1} h^{-1} [33]), $m_{\text{ref,th}}$ is the reference mass of the thyroid (20.7 g), and m_s is the site mass.

As shown, the S-values used in Eq. (7) are slightly higher than the unit-density sphere S-values, used in whole-volume dosimetry (Method 1), although differences are subtle. Voxel-based S-values, used in maximum-voxel dosimetry (Method 2), are slightly lower, with increasing differences as the mass increases. When including the contribution from the neighboring voxels, the S-values are nearly identical.

Another reason for the observed differences between whole-volume and maximum-voxel dosimetry is the integration of the time-activity values to cumulated activity. As seen in Fig. 2, the activity concentrations for each time-point are consistent, but even small deviations from the identity line in each SPECT/CT acquisition can result in large differences in effective half-lives as shown in Fig. 3, especially for higher effective half-lives. In this study, it was not feasible to perform the third acquisition in the same day for all patients, but the differences in the effective half-lives between Methods 1 and 2 did not correlate with the day of the third acquisition. Thus, any extra time-point acquired during the washout phase would help to achieve less variability in the effective half-lives between Methods 1 and 2.

There is an increased evidence in radionuclide therapy of a dose-effect correlation.[34] In DTC treatments, dose-effect correlations have been reported but there is no consensus on the remnant absorbed dose above which there is a higher probability to achieve a successful ablation.[11,14,18] If the administered activity could be tailored to reach a predefined absorbed dose to thyroid remnants, adequate for successful ablation, then excess levels of ^{131}I-NaI could be avoided, thus minimizing the probability of unwanted side-effects, such as sialadenitis and xerostomia[35] and second primary cancers.[36,37] In addition, the number of patients with recurring or persistent disease, which can entail the loss of iodine avidity, could possibly be minimized.[38] A reduction of the administered activity would also be clearly beneficial for the radiological protection of caregivers and comforters. Pretreatment dosimetry with a tracer may be considered an increased economic cost of the treatment. However, Maxon *et al.*[13] showed that tailoring the absorbed dose to the individual patient may in many cases decrease the administered amount of activity. This may reduce the hospitalization time, and some treatments could even be performed on an outpatient basis, thereby decreasing the overall cost of the treatment. The administration of a tracer has been reported to cause the so-called thyroid stunning.[39,40] Lassmann *et al.*,[16] recommended not to administer any amount of ^{131}I before treatment because its uptake was notably reduced after administering a tracer of 74 MBq. However, this effect is still unclear[41] and it has been explained as a reduced expression of NIS (Ref. 42) or alternatively as a result of cell killing.[43] In order to avoid the stunning effect, the use of ^{124}I as a tracer (decays modes are electron capture and positron emission) seems a promising alternative because the self-irradiation of the remnant would be avoided.[20] Further dosimetric studies on this subject are thus warranted. The dosimetric method used in this study can be implemented at most centers treating DTC, relying only on the availability of SPECT/CT scanning, access to basic quality-control phantoms and software to analyze DICOM images. Future dose–response correlation studies may need to take into account the disease stage, the thyroid remnants mass left after surgery,[14] and the patient preparation before treatment, including the protocols for surgery and hormone withdrawal or stimulation with rhTSH.[44]

5. CONCLUSIONS

In this study, SPECT/CT dosimetry in DTC patients, based on the whole-remnant and the maximum-voxel, is described and compared. Generally, consistent absorbed doses are obtained from the two methods, although the maximum-voxel method yields values that are on average 20% lower than the whole-remnant method due to differences in the S-values. In some cases, differences also result from the estimated effective half-lives, indicating that additional acquisition time-points are warranted. Practically, for the future, either of the dosimetry methods is useful. In order to rule out the difference related to the S-values, the absorbed dose derived from the maximum-voxel method would need to be multiplied by a factor dependent on remnant mass, which can be as high as 1.2.

ACKNOWLEDGMENT

This work was supported by the Swedish Research Council (Grant No. 621-2014-6187), the Berta Kamprad Foundation, and the Gunnar Nilsson Cancer Foundation.

CONFLICT OF INTEREST DISCLOSURE

The authors have no COI to report.

APPENDIX A: OBTENTION OF THE SITE VOLUME FROM RECOVERY COEFFICIENTS

This section is included to show that, given the assumption of homogenous activity concentration, recovery coefficients are applicable for both whole-volume and maximum-voxel dosimetry.

For a spherical object with volume v_o and homogenous activity concentration $[A]$, the contained activity is given by

$$A = [A]v_o. \tag{A1}$$

If this object is imaged by an ideal system, i.e., with ideal spatial resolution, the activity can be described as

$$A = \frac{1}{\varepsilon}C_t = \frac{1}{\varepsilon}c_o N_o, \tag{A2}$$

where C_t is the total count rate in the object, c_o is the count rate per voxel, and N_o is the number of object voxels. The object volume is given by

$$v_o = \Delta v N_o = \Delta v \frac{C_t}{c_o}, \tag{A3}$$

where Δv is the voxel volume. In a real imaging system, the limited spatial resolution affects the count distribution. For a sphere with a diameter large in comparison with the FWHM of the PSF, the maximum voxel count-rate, c_m, gives a good estimate of c_o, i.e., the voxel count-rate in absence of resolution effects. The volume v_o is then approximately equal to the apparent object volume, v_a, i.e., the volume as measured in the image when it is affected by limited spatial resolution,

$$v_a = \Delta v \frac{C_t}{c_m}. \tag{A4}$$

For smaller spheres, limited by the spatial resolution, c_m underestimates c_o, while v_a overestimates v_o. In Appendix B, v_a are shown, when estimated using Eq. (A4), as function of v_o for simulated data and different spatial resolutions.

The recovery coefficient, RC, is defined as the ratio of the measured and true activity concentrations. Following the above equations, the RC describes the ratio of count rates or volumes (see Appendix C) according to

$$\mathrm{RC} = \frac{c_m}{c_o} = \frac{v_o}{v_a}. \tag{A5}$$

Appendix B shows RCs for simulated data and different spatial resolutions, as function of both the true and the apparent sphere volumes.

For analysis of the patient SPECT images in this study, the RC was determined from the IEC phantom data by determining v_a according to Eq. (A4) and applying Eq. (A5), i.e., the ratio of the true and apparent sphere volumes. Figure 7 shows the experimentally determined RC. In order to interpolate between data points, an equation was fitted to the RC-versus-v_a data, taking the SDs into account, using the following sigmoid function:

$$\mathrm{RC}(v_a) = \frac{1}{1+\exp(-\alpha(v_a-\beta))}, \tag{A6}$$

where α and β are fit parameters.

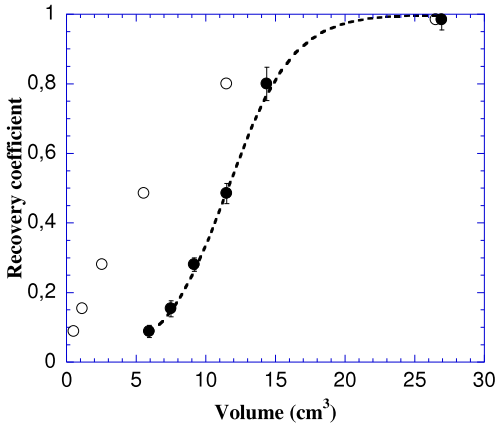

FIG. 7. Experimentally determined recovery coefficients (RCs) from the IEC phantom data. Open symbols show RCs as function of true sphere volume, whereas filled symbols are RCs as function of the apparent volumes. Dashed line is a fitted expression in Eq. (A6).

APPENDIX B: VALUES OF RECOVERY COEFFICIENTS FROM COMPUTER SIMULATIONS

Figure 8 shows results of computer simulations mimicking the effect of different spatial resolutions. It is seen that the overestimate in the apparent volume, v_a, for small volumes is more pronounced when the spatial resolution is poor. For

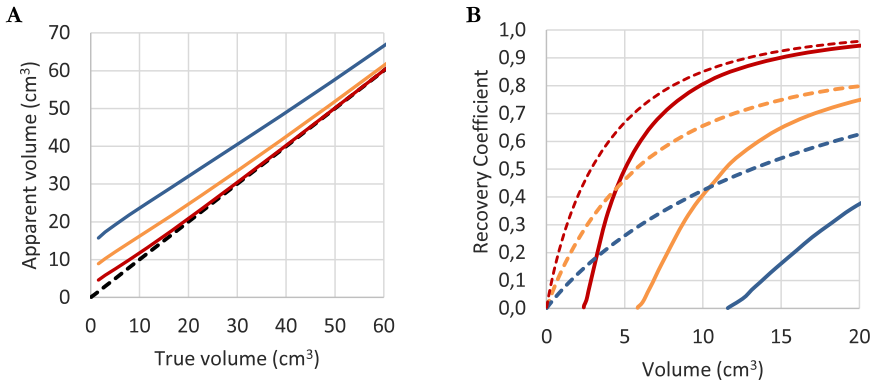

FIG. 8. Results from computer simulations for FWHMs of 13.3 mm (red), 17.7 mm (green), and 22.1 mm (blue). (A) The apparent volume, v_a, obtained by application of Eq. (A4), as function of true sphere volumes, v_o. Identity line is dashed. (B) Recovery coefficients, determined using Eq. (A6), plotted both versus true sphere volumes (dashed lines) and apparent volumes (solid lines). (See color online version.)

larger volumes, v_a converges toward v_o, and the recovery coefficient converges to a value of 1.

APPENDIX C: ACTIVITY PER VOXEL

The recovery coefficient, RC, in Eq. (A5), is described as

$$\mathrm{RC} = \frac{[A]_{\mathrm{meas}}}{[A]_{\mathrm{true}}} = \frac{A/v_a}{A/v_o} = \frac{v_o}{v_a} = \frac{c_m}{c_o}. \quad \text{(C1)}$$

The expression for the activity per voxel in Eq. (5) is derived according to

$$A_{\mathrm{vx}} = [A]\Delta v = \frac{A}{v_o}\Delta v = \frac{1}{\varepsilon}\frac{C_t}{v_o}\Delta v = \frac{1}{\varepsilon}\frac{c_o}{\Delta v}\Delta v = \frac{1}{\varepsilon}\frac{c_m}{\mathrm{RC}(v_a)}. \quad \text{(C2)}$$

[a]Author to whom correspondence should be addressed. Electronic mail: pablo.minguezgabina@osakidetza.eus; Telephone: +34 94 600 61 73.

[1]E. B. Silberstein, A. Alavi, H. R. Balon, S. E. Clarke, C. Divgi, M. J. Gelfand, S. J. Goldsmith, H. Jadvar, C. S. Marcus, W. H. Martin, J. A. Parker, H. D. Royal, S. D. Sarkar, M. Stabin, and A. D. Waxman, "The SNMMI practice guideline for therapy of thyroid disease with ^{131}I 3.0," J. Nucl. Med. **53**, 1633–1651 (2012).

[2]M. Luster, S. E. Clarke, M. Dietlein, M. Lassmann, P. Lind, W. J. Oyen, J. Tennvall, and E. Bombardieri, European Association of Nuclear Medicine, "Guidelines for radioiodine therapy of differentiated thyroid cancer," Eur. J. Nucl. Med. Mol. Imaging **35**, 1941–1959 (2008).

[3]P. W. Rosario, A. L. Barroso, L. L. Rezende, E. L. Padrao, T. A. Fagundes, J. S. Reis, and S. Purisch, "Outcome of ablation of thyroid remnants with 100 mCi (3.7 GBq) iodine-131 in patients with thyroid cancer," Ann. Nucl. Med. **19**, 247–250 (2005).

[4]T. Pilli, E. Brianzoni, F. Capoccetti, M. G. Castagna, S. Fattori, A. Poggiu, G. Rossi, F. Ferretti, E. Guarino, L. Burroni, A. Vattimo, C. Cipri, and F. Pacini, "A comparison of 1850 (50 mCi) and 3700 MBq (100 mCi) 131-iodine administered doses for recombinant thyrotropin-stimulated postoperative thyroid remnant ablation in differentiated thyroid cancer," J. Clin. Endocrinol. Metab. **92**, 3542–3546 (2007).

[5]M. Schlumberger, B. Catargi, I. Borget, D. Deandreis, S. Zerdoud, B. Bridji, S. Bardet, L. Leenhardt, D. Bastie, C. Schvartz, P. Vera, O. Morel, D. Benisvy, C. Bournaud, F. Bonichon, C. Dejax, M. E. Toubert, S. Leboulleux, M. Ricard, and E. Benhamou, Tumeurs de la Thyroide Refractaires Network for the Essai Stimulation Ablation Equivalence Trial, "Strategies of radioiodine ablation in patients with low-risk thyroid cancer," N. Engl. J. Med. **366**, 1663–1673 (2012).

[6]C. C. Kuni and W. C. Klingensmith III, "Failure of low doses of ^{131}I to ablate residual thyroid tissue following surgery for thyroid cancer," Radiology **137**, 773–774 (1980).

[7]A. Kukulska, J. Krajewska, M. Gawkowska-Suwinska, Z. Puch, E. Paliczka-Cieslik, J. Roskosz, D. Handkiewicz-Junak, M. Jarzab, E. Gubala, and B. Jarzab, "Radioiodine thyroid remnant ablation in patients with differentiated thyroid carcinoma (DTC): Prospective comparison of long-term outcomes of treatment with 30, 60, and 100 mCi," Thyroid Res. **3**, 9–12 (2010).

[8]A. Hackshaw, C. Harmer, U. Mallick, M. Haq, and J. A. Franklyn, "^{131}I activity for remnant ablation in patients with differentiated thyroid cancer: A systematic review," J. Clin. Endocrinol. Metab. **92**, 28–38 (2007).

[9]N. Arslan, S. Ilgan, M. Serdengecti, M. A. Ozguven, H. Bayhan, K. Okuyucu, and S. A. Gulec, "Post-surgical ablation of thyroid remnants with high-dose (131)I in patients with differentiated thyroid carcinoma," Nucl. Med. Commun. **22**, 1021–1027 (2001).

[10]S. J. Goldsmith, "To ablate or not to ablate: Issues and evidence involved in ^{131}I ablation of residual thyroid tissue in patients with differentiated thyroid carcinoma," Semin. Nucl. Med. **41**, 96–104 (2011).

[11]H. R. Maxon, S. R. Thomas, V. S. Hertzberg, J. G. Kereiakes, I. W. Chen, M. I. Sperling, and E. L. Saenger, "Relation between effective radiation dose and outcome of radioiodine therapy for thyroid cancer," N. Engl. J. Med. **309**, 937–941 (1983).

[12]K. F. Koral, R. S. Adler, J. E. Carey, and W. H. Beierwaltes, "Iodine-131 treatment of thyroid cancer: Absorbed dose calculated from post-therapy scans," J. Nucl. Med.: Off. Publ., Soc. Nucl. Med. **27**, 1207–1211 (1986).

[13]H. R. Maxon III, E. E. Englaro, S. R. Thomas, V. S. Hertzberg, J. D. Hinnefeld, L. S. Chen, H. Smith, D. Cummings, and M. D. Aden, "Radioiodine-131 therapy for well-differentiated thyroid cancer–a quantitative radiation dosimetric approach: Outcome and validation in 85 patients," J. Nucl. Med.: Off. Publ., Soc. Nucl. Med. **33**, 1132–1136 (1992).

[14]M. E. O'Connell, M. A. Flower, P. J. Hinton, C. L. Harmer, and V. R. McCready, "Radiation dose assessment in radioiodine therapy. Dose-response relationships in differentiated thyroid carcinoma using quantitative scanning and PET," Radiother. Oncol.: J. Eur. Soc. Ther. Radiol. Oncol. **28**, 16–26 (1993).

[15]A. M. Samuel and B. Rajashekharrao, "Radioiodine therapy for well-differentiated thyroid cancer: A quantitative dosimetric evaluation for remnant thyroid ablation after surgery," J. Nucl. Med.: Off. Publ., Soc. Nucl. Med. **35**, 1944–1950 (1994).

[16]M. Lassmann, M. Luster, H. Hanscheid, and C. Reiners, "Impact of ^{131}I diagnostic activities on the biokinetics of thyroid remnants," J. Nucl. Med.: Off. Publ., Soc. Nucl. Med. **45**, 619–625 (2004).

[17]F. Capoccetti, B. Criscuoli, G. Rossi, F. Ferretti, C. Manni, and E. Brianzoni, "The effectiveness of ^{124}I PET/CT in patients with differentiated thyroid cancer," Q. J. Nucl. Med. Mol. Imaging: Off. Publ. Ital. Assoc. Nucl. Med. **53**, 536–545 (2009).

[18]G. D. Flux, M. Haq, S. J. Chittenden, S. Buckley, C. Hindorf, K. Newbold, and C. L. Harmer, "A dose–effect correlation for radioiodine ablation in differentiated thyroid cancer," Eur. J. Nucl. Med. Mol. Imaging **37**, 270–275 (2010).

[19]P. Minguez, J. Genolla, J. J. Celeiro, and J. C. Fombellida, "Dosimetry in differentiated thyroid carcinoma (12–1402R)," Med. Phys. **40**, 012502 (7pp.) (2013).

[20]W. Jentzen, A. S. Moldovan, M. Ruhlmann, R. Gorges, A. Bockisch, and S. Rosenbaum-Krumme, "Lowest effective ^{131}I activity for thyroid remnant ablation of differentiated thyroid cancer patients. Dosimetry-based model for estimation," Nuklearmedizin **54**, 137–143 (2015).
[21]International Atomic Energy Agency, "Release of patients after radionuclide therapy," Safety Report Series No. 63, IAEA, Vienna, 2009.
[22]International Electrotechnical Commission, "Radionuclide imaging devices—Characteristics and test conditions. Part I. Positron emission tomographs," IEC 61675-1, IEC, Geneva, 2008.
[23]M. G. Stabin and M. W. Konijnenberg, "Re-evaluation of absorbed fractions for photons and electrons in spheres of various sizes," J. Nucl. Med.: Off. Publ., Soc. Nucl. Med. **41**, 149–160 (2000).
[24]A. Dieudonne, R. F. Hobbs, R. Lebtahi, F. Maurel, S. Baechler, R. L. Wahl, A. Boubaker, D. Le Guludec, G. Sgouros, and I. Gardin, "Study of the impact of tissue density heterogeneities on 3-dimensional abdominal dosimetry: Comparison between dose kernel convolution and direct Monte Carlo methods," J. Nucl. Med.: Off. Publ., Soc. Nucl. Med. **54**, 236–243 (2013).
[25]ICRP, "Basic anatomical and physiological data for use in radiological protection reference values. ICRP Publication 89," Ann. ICRP **32**(3-4), 225–227 (2002).
[26]N. Lanconelli, M. Pacilio, S. Lo Meo, F. Botta, A. Di Dia, A. T. Aroche, M. A. Perez, and M. Cremonesi, "A free database of radionuclide voxel S values for the dosimetry of nonuniform activity distributions," Phys. Med. Biol. **57**, 517–533 (2012).
[27]M. R. Nadig, G. S. Pant, and C. Bal, "Usefulness of ^{99}mTc-pertechnetate single-photon emission computed tomography in remnant mass estimation of postsurgical patients of differentiated thyroid cancer during internal dosimetry," Nucl. Med. Commun. **29**, 809–814 (2008).
[28]G. DiRusso and K. A. Kern, "Comparative analysis of complications from I-131 radioablation for well-differentiated thyroid cancer," Surgery **116**, 1024–1030 (1994).
[29]M. Braga, M. D. Ringel, and D. S. Cooper, "Sudden enlargement of local recurrent thyroid tumor after recombinant human TSH administration," J. Clin. Endocrinol. Metab. **86**, 5148–5151 (2001).
[30]V. E. Nielsen, S. J. Bonnema, and L. Hegedus, "Effects of 0.9 mg recombinant human thyrotropin on thyroid size and function in normal subjects: A randomized, double-blind, cross-over trial," J. Clin. Endocrinol. Metab. **89**, 2242–2247 (2004).
[31]M. Luster, F. Lippi, B. Jarzab, P. Perros, M. Lassmann, C. Reiners, and F. Pacini, "rhTSH-aided radioiodine ablation and treatment of differentiated thyroid carcinoma: A comprehensive review," Endocr.-Relat. Cancer **12**, 49–64 (2005).
[32]D. M. Howard, K. J. Kearfott, S. J. Wilderman, and Y. K. Dewaraja, "Comparison of I-131 radioimmunotherapy tumor dosimetry: Unit density sphere model versus patient-specific Monte Carlo calculations," Cancer biother. Radiopharm. **26**, 615–621 (2011).
[33]W. S. Snyder, M. R. Ford, G. G. Warner, and S. B. Watson, *MIRD Pamphlet #11: S, Absorbed Dose Per Unit Cumulated Activity for Selected Radionuclides and Organs* (Society of Nuclear Medicine, Reston, 1975).
[34]L. Strigari, M. Konijnenberg, C. Chiesa, M. Bardies, Y. Du, K. S. Gleisner, M. Lassmann, and G. Flux, "The evidence base for the use of internal dosimetry in the clinical practice of molecular radiotherapy," Eur. J. Nucl. Med. Mol. Imaging **41**, 1976–1988 (2014).
[35]S. Y. Jeong, H. W. Kim, S. W. Lee, B. C. Ahn, and J. Lee, "Salivary gland function 5 yr after radioactive iodine ablation in patients with differentiated thyroid cancer: Direct comparison of pre- and post-ablation scintigraphies and their relation to xerostomia symptoms," Thyroid: Off. J. Am. Thyroid Assoc. **23**, 609–616 (2013).
[36]E. Berthe, M. Henry-Amar, J. J. Michels, J. P. Rame, P. Berthet, E. Babin, P. Icard, G. Samama, F. Galateau-Salle, J. Mahoudeau, and S. Bardet, "Risk of second primary cancer following differentiated thyroid cancer," Eur. J. Nucl. Med. Mol. Imaging **31**, 685–691 (2004).
[37]G. H. Seo, Y. Y. Cho, J. H. Chung, and S. W. Kim, "Increased risk of leukemia after radioactive iodine therapy in patients with thyroid cancer: A nationwide, population-based study in Korea," Thyroid: Off. J. Am. Thyroid Assoc. **25**, 927–934 (2015).
[38]N. L. Busaidy and M. E. Cabanillas, "Differentiated thyroid cancer: Management of patients with radioiodine nonresponsive disease," J. Thyroid Res. **2012**, 618985.
[39]R. W. Rawson, J. E. Rall, and W. Peacock, "Limitations and indications in the treatment of cancer of the thyroid with radioactive iodine," J. Clin. Endocrinol. Metab. **11**, 1128–1142 (1951).
[40]H. M. Park, Y. H. Park, and X. H. Zhou, "Detection of thyroid remnant/metastasis without stunning: An ongoing dilemma," Thyroid: Off. J. Am. Thyroid Assoc. **7**, 277–280 (1997).
[41]I. R. McDougall and A. Iagaru, "Thyroid stunning: Fact or fiction?," Semin. Nucl. Med. **41**, 105–112 (2011).
[42]M. M. Norden, F. Larsson, S. Tedelind, T. Carlsson, C. Lundh, E. Forssell-Aronsson, and M. Nilsson, "Down-regulation of the sodium/iodide symporter explains ^{131}I-induced thyroid stunning," Cancer Res. **67**, 7512–7517 (2007).
[43]S. Walrand, M. Hesse, and F. Jamar, "Statistical and radiobiological analysis of the so-called thyroid stunning," EJNMMI Res. **5**, 67–72 (2015).
[44]H. Hanscheid, M. Lassmann, M. Luster, S. R. Thomas, F. Pacini, C. Ceccarelli, P. W. Ladenson, R. L. Wahl, M. Schlumberger, M. Ricard, A. Driedger, R. T. Kloos, S. I. Sherman, B. R. Haugen, V. Carriere, C. Corone, and C. Reiners, "Iodine biokinetics and dosimetry in radioiodine therapy of thyroid cancer: Procedures and results of a prospective international controlled study of ablation after rhTSH or hormone withdrawal," J. Nucl. Med.: Off. Publ., Soc. Nucl. Med. **47**, 648–654 (2006).